

ATLAS: Adaptive Topology-based Learning at Scale for Homophilic and Heterophilic Graphs

Turja Kundu
 University of North Texas
 Denton, Texas, USA
 turjakundu@my.unt.edu

Sanjukta Bhowmick
 University of North Texas
 Denton, Texas, USA
 sanjukta.bhowmick@unt.edu

Abstract

Graph neural networks (GNNs) excel on homophilic graphs where connected nodes share labels, but struggle with heterophilic graphs where edges do not imply similarity. Moreover, iterative message passing limits scalability due to neighborhood expansion overhead. We introduce ATLAS (Adaptive Topology-based Learning at Scale), a propagation-free framework that encodes graph structure through multi-resolution community features rather than message passing.

We first prove that community refinement involves a fundamental trade-off: finer partitions increase label-community mutual information but also increase entropy. We formalize when refinement improves normalized mutual information, explaining why intermediate granularities are often most predictive. ATLAS employs modularity-guided adaptive search to automatically identify informative community scales, which are then one-hot encoded, projected into learnable embeddings, and concatenated with node attributes for MLP classification. This enables standard mini-batch training and adjacency-free inference after one-time preprocessing.

Across 13 benchmarks including million-node graphs, ATLAS achieves competitive or superior accuracy—up to 20-point gains over GCN on heterophilic datasets and 12-point gains over MLPs on homophilic graphs. By treating topology as explicit features, ATLAS adapts intelligently: leveraging structure when informative, remaining robust when weakly aligned, and avoiding propagation when structure misleads, providing both scalable performance and interpretable structural insights.

Keywords

graph learning, community, heterophily, homophily, scalable training

ACM Reference Format:

Turja Kundu and Sanjukta Bhowmick. 2026. ATLAS: Adaptive Topology-based Learning at Scale for Homophilic and Heterophilic Graphs. In . ACM, New York, NY, USA, 17 pages.

1 Introduction

Node classification, a fundamental problem in graph learning, involves identifying labels of nodes in a graph and has wide applications in many domains including social networks, citation networks, recommendation systems, knowledge graphs and bioinformatics [17, 38, 46]. Accurate classification requires two complementary pieces of information—(i) the features at each node, and (ii) the connections between the node and its neighbors. Neural

network methods such as Multi-Layer Perceptrons (MLPs) are fast but do not include information about the connections. Graph Neural Networks (GNNs) address this problem by aggregating the features between neighboring nodes, but the process is expensive and difficult to scale to large graphs. To improve scalability, sampling-based methods construct mini-batches by sampling neighborhoods or subgraphs (e.g., ClusterGCN, GraphSAGE, GraphSAINT) [6, 11, 44]; however, this introduces an additional granularity choice—the fan-out or subgraph/cluster size—that trades off computational cost against how much structural context is captured per update. Although the graph structure can be represented as feature vectors using different node embedding techniques [10, 26, 34], or through the use of community-aware representations/features derived from community detection [16, 32], the issue remains as to how many hops of neighbors should be considered and how fine-grained the communities (or sampled subgraphs) should be. Larger hops, larger sampled subgraphs, or coarse-grained communities can lead to information smoothing, while smaller hops, smaller sampled subgraphs, or fine-grained communities can lead to information loss. Further, the hypothesis that aggregating features of neighbors can improve accuracy of node classification is only true for homophilic networks (where nodes of similar classes are connected). In heterophilic networks, where the connection between nodes need not imply similarity of class, this strategy leads to lower accuracy. Based on these observations, we posit that *matching structural information (i.e., size of hops, sampled subgraphs/clusters, or communities) with how well it aligns with the classification task is necessary for producing accurate results*.

1.1 Our Proposed Method: ATLAS

Current graph learning approaches face a critical trade-off. Most methods either (i) work well only on homophilic graphs where connected nodes tend to share labels, or (ii) handle heterophily through computationally expensive mechanisms—signal modification, graph rewiring, or spectral objectives—that struggle to scale to large graphs. Compounding this challenge, commonly used homophily or heterophily metrics (e.g., edge homophily) are often insufficient to characterize whether graph structure is informative for a given learning task. Recent studies show that similar homophily scores can correspond to very different GNN performance, and that low homophily does not imply uninformative topology [27, 28, 47].

Our Solution. To address this challenge, we present ATLAS (Adaptive Topology-based Learning at Scale), a scalable framework that delivers strong performance across both medium-sized and million-node benchmarks, regardless of whether the graph exhibits

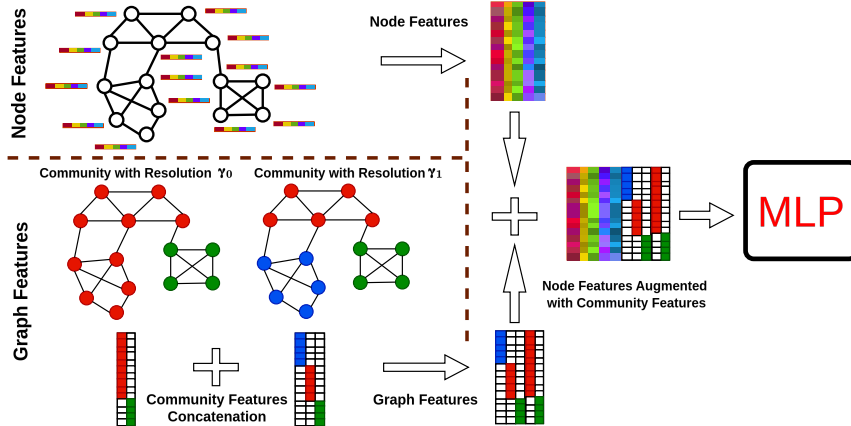


Figure 1: Overview of the community-augmented feature learning pipeline. Community assignments at multiple resolutions are one-hot encoded, projected, concatenated with node features, and input to an MLP for classification.

homophily or heterophily. ATLAS either achieves the best performance or comes within 1% of the best method across diverse structural (heterophilic or homophilic) regimes (exceptions are Roman-Empire 5.5% and Ogbn-products 3.5%).

Core Innovation. ATLAS fundamentally rethinks how to inject structural information into graph learning by *treating topology as an explicit, controllable signal*. Rather than relying on iterative message passing, we extract multi-resolution community structure and use it directly as topology features. The approach is straightforward, we compute community assignments at multiple granularities, encode these assignments, and concatenate them with node attributes before training a compact MLP. This topology-as-features design enables propagation-free training and inference after preprocessing, while still capturing essential meso-scale structural context.

Making topology explicit also opens a *new path to interpretability*. While existing GNN explanation methods (GNNExplainer, PGExplainer, SubgraphX) provide post-hoc subgraph attributions [15, 23, 40, 42], ATLAS offers a direct "granularity knob"—each feature block corresponds to community membership at a specific resolution, letting practitioners immediately see which structural scales matter most for their task and how accuracy responds across granularities.

In summary, our contributions are:

- (1) **Theoretical Analysis of Community Refinement.** We provide a theoretical analysis of how community refinement affects label-community alignment measured by NMI and explain why intermediate granularities can be most informative. This analysis reveals the fundamental trade-off between alignment and entropy that creates optimal structural scales for prediction (Section 2).
- (2) **Adaptive Topology Encoding.** We introduce ATLAS, a scalable topology encoder that represents graph structure through learnable community features across multiple resolutions, integrated with a lightweight MLP for node classification. Our unsupervised, modularity-guided adaptive search automatically identifies a small set of informative community

resolutions and converts their assignments into topology features, eliminating the need for manual tuning or labeled data (Section 3).

- (3) **Comprehensive Evaluation.** We evaluate ATLAS on 13 graphs (8 medium-scale and 5 large-scale) spanning both homophilic and heterophilic settings, comparing against 14 medium-scale and 9 large-scale GNN/MLP baselines. Through extensive ablations and structural-bias analyses, we demonstrate that ATLAS narrows the MLP-GNN accuracy gap while preserving high efficiency (Sections 4–5).

2 Theoretical Analysis

We provide a theoretical justification for why community refinement at different resolutions improves classification accuracy. Consider the progression illustrated in Figure 2: initially, two communities each contain a mixture of both classes (triangles and squares), yielding accuracy no better than random guessing (top). As these communities are refined, clusters become more homogeneous with respect to class labels, and accuracy improves (middle). However, excessive refinement proves counterproductive. Overly small communities fragment class information, degrading predictive power (bottom). This reveals a critical insight. **Only communities with high normalized mutual information (NMI) between structure and labels should be retained.** As refinement progresses and NMI declines, those communities should be excluded from the feature set. We formalize this intuition through a series of theorems, with complete proofs provided in the appendix.

Let N be the set of nodes. Let $P = \{P_1, \dots, P_k\}$ be a partition of N ; i.e.

$$P_i \neq \emptyset, \quad P_i \cap P_j = \emptyset \ (i \neq j), \quad \text{and} \quad \bigcup_{i=1}^k P_i = N.$$

Let $S = \{S_1, \dots, S_m\}$ be another partition of N . We say S is a refinement of P (denoted as $S \preceq P$) iff every block of S is contained in some block of P . Formally:

$$S \preceq P \iff \forall S_j \in S \ \exists P_i \in P \text{ such that } S_j \subseteq P_i.$$

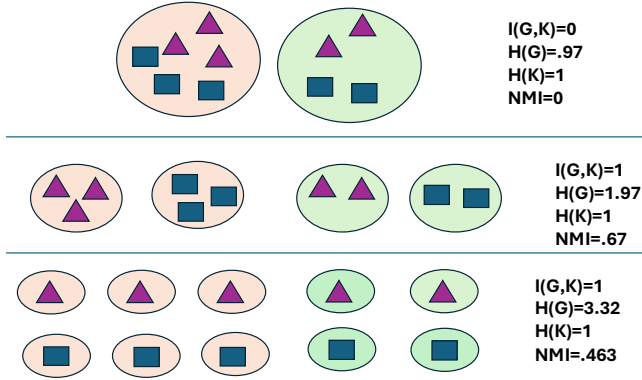


Figure 2: Effect of refinement on NMI. Initially when clusters have mixed items, NMI is low. The first refinement matches the items and clusters, increasing the NMI. Further refinement does not improve the alignment (mutual information), but increases the spread (entropy), thus decreasing NMI.

Normalized mutual information (NMI) is a popular measure to quantify alignment between two partitions. Given two partitions P and Q , over a set of N elements and $n_{ij} = |P_i \cap Q_j|$, $n_i = |P_i|$, $n_j = |Q_j|$ their normalized mutual information is given as:

$$NMI(P, Q) = \frac{2I(P; Q)}{H(P) + H(Q)}$$

$I(P, Q) = \sum_{i=1}^k \sum_{j=1}^m \frac{n_{ij}}{N} \log \left(\frac{N n_{ij}}{n_i n_j} \right)$ is the mutual information between partitions P and Q . This quantity measures how much information is shared between the partitions P and Q . The higher the value, the better the alignment between the partitions. $H(P) = -\sum_{i=1}^k \frac{n_i}{N} \log \left(\frac{n_i}{N} \right)$, is the entropy of partition P . $H(Q)$ is defined similarly. The entropy measures the distribution of points in each partition. Low entropy means data is concentrated in few clusters, and is indicative of good clustering.

The value of NMI ranges from 1 (indicating complete alignment between partitions) to close to 0 (indicating complete mismatch between partitions). NMI is high if the partitions are well matched ($I(P, Q)$ is high), and entropy is low ($H(P), H(Q)$ is low).

LEMMA 1 (REFINEMENT DOES NOT DECREASE MUTUAL INFORMATION). Let L be labels and C a community partition. Let C' be a refinement of C , i.e., $C' \preceq C$. Then $I(L; C') \geq I(L; C)$

LEMMA 2 (REFINEMENT DOES NOT DECREASE ENTROPY). Let C a community partition. Let C' be a refinement of C , i.e., $C' \preceq C$. Then $H(C') \geq H(C)$

Based on Lemma 1 and Lemma 2 we see that while refinement improves the mutual information leading to better alignment, it also increases the entropy leading to more noise or uncertainty. The condition at which NMI will increase is given by Theorem 1.

THEOREM 1 (NMI REFINEMENT CONDITION). Let L be labels; C a community partition. Let C' be a refinement of C , i.e., $C' \preceq C$. Then

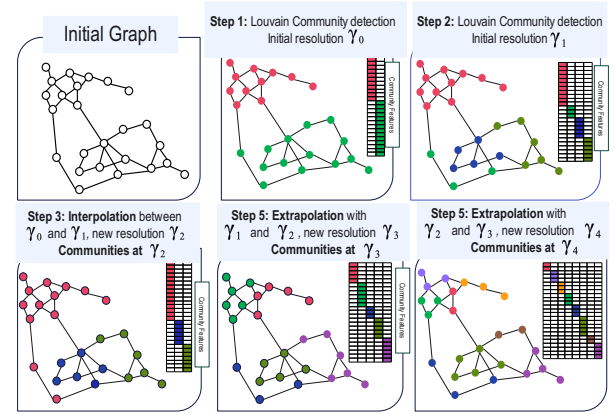


Figure 3: Illustration of the Adaptive Resolution Search Process. The resolution limits, $\gamma_0 < \gamma_2 < \gamma_1 < \gamma_3 < \gamma_4$, and the communities $C^{\gamma_0} \preceq C^{\gamma_2} \preceq C^{\gamma_1} \preceq C^{\gamma_3} \preceq C^{\gamma_4}$ capture structural bias for different granularities from the graph.

$$NMI(C'; L) > NMI(C; L) \quad \text{if and only if} \quad \frac{\Delta I}{\Delta H} > \frac{NMI(C; L)}{2}, \text{ where} \\ \Delta I = I(C'; L) - I(C; L) \text{ and } \Delta H = H(C'; L) - H(C; L)$$

Theorem 1 states that a partition refinement improves the normalized mutual information with respect to labels if and only if the mutual information gain per unit of entropy increase exceeds half the original normalized mutual information value.

3 Methodology

Section 2 analyzes community refinement under idealized assumptions, where refined communities form perfect nested subsets of coarser ones—a hierarchical structure that guarantees theoretical properties. In practice, however, we must adapt this framework to work with real-world community detection algorithms.

We approximate refinement by running Louvain at multiple values of its resolution parameter γ . Increasing γ typically yields finer partitions. However, two key challenges arise in practice. *First*, the resulting partitions are not guaranteed to be strictly nested due to Louvain’s heuristic optimization and non-determinism. *Second*, varying degrees of homophily across the datasets mean that refining communities does not always increase the homogeneity of class labels. To bridge this gap between theory and practice while avoiding the computational cost of sweeping a dense grid of γ values, ATLAS performs an *adaptive resolution search* (Algorithm 1 in the appendix) during preprocessing that identifies a small set of informative resolutions. By computing community assignments only at these carefully selected resolutions, we achieve an efficient approximation of the idealized refinement structure that adapts to the structural properties of each graph.

Notation. For a resolution γ , Louvain returns a node-to-community assignment $c^{(\gamma)}$ and its modularity score $Q^{(\gamma)}$. Modularity Q measures the strength of within-community connectivity relative to a null model with randomly placed edges. Given two values $\gamma_1 < \gamma_2$, we define the modularity gap as $\Delta Q(\gamma_1, \gamma_2) = |Q^{(\gamma_2)} - Q^{(\gamma_1)}|$.

Appendix A.1 provides additional community terminology and formal definitions. We define the steps of our algorithm below:

Preprocessing: Adaptive Resolution Search. The adaptive search algorithm starts from an initial set of resolution values $\gamma \in \{0.5, 1.0\}$ (Γ_0 can include smaller values like $\gamma \in [0, 0.5]$ for graphs with informative structure at low resolution) and iteratively refines this set using three hyperparameters: *a maximum modularity-gap threshold Δ_{\max} , a minimum modularity threshold Q_{\min} , and a target range for modularity decrease $[a, b]$* .

At each iteration, the algorithm sorts γ and examines neighboring resolution pairs (γ_1, γ_2) employing **two strategies** to refine the search. When a pair exhibits a modularity gap $\Delta Q(\gamma_1, \gamma_2) > \Delta_{\max}$, the algorithm performs **interpolation** by inserting the midpoint between them to better capture sharp structural transitions. Conversely, when all neighboring gaps fall within acceptable bounds, it performs **extrapolation** by extending beyond the current maximum γ , selecting a step size that reduces modularity by an amount sampled from $[a, b]$ based on the observed trend of $Q^{(\gamma)}$ across Γ . The process terminates once modularity at the largest γ drops below Q_{\min} or when no new resolution values are generated. The algorithm outputs the refined resolution set Γ and the corresponding community assignments $\{c^{(\gamma)}\}_{\gamma \in \Gamma}$, which serve as multi-resolution community features for subsequent encoding and concatenation with node features during the feature augmentation step.

Feature Augmentation. For a resolution $\gamma \in \Gamma$, community detection on G yields node assignments $c^{(\gamma)} \in \{1, \dots, k_{\gamma}\}^n$. We one-hot encode them as $H^{(\gamma)}$ ((2)) and project to a dense space using a trainable $W^{(\gamma)}$ ((3)). Concatenating embeddings across resolutions forms E ((4)), which is concatenated with node features X to obtain Z_{ATLAS} . An MLP f_{θ} outputs logits, and a task-dependent map ϕ (e.g., softmax or elementwise sigmoid) produces probabilities \hat{Y} ((6)).

$$c^{(\gamma)} = \text{DetectCommunity}(G, \gamma), \quad c^{(\gamma)} \in \{1, \dots, k_{\gamma}\}^n \quad (1)$$

$$H^{(\gamma)} = \text{OneHot}(c^{(\gamma)}) \in \{0, 1\}^{n \times k_{\gamma}} \quad (2)$$

$$E^{(\gamma)} = H^{(\gamma)} W^{(\gamma)}, \quad W^{(\gamma)} \in \mathbb{R}^{k_{\gamma} \times d} \quad (3)$$

$$E = \big\|_{t=1}^T E^{(t)} \in \mathbb{R}^{n \times (Td_c)} \quad (4)$$

$$Z_{\text{ATLAS}} = [X \parallel E] \in \mathbb{R}^{n \times (D+Td_c)} \quad (5)$$

$$\hat{Y} = \phi(f_{\theta}(Z_{\text{ATLAS}})) \in [0, 1]^{n \times C}. \quad (6)$$

Complexity Analysis. We compare the preprocessing, training, and inference complexity of ATLAS to representative GNN and scalable baselines. As summarized in Table 3, ATLAS incurs a one-time community-detection cost of $O(T\|A\|_0)$ to extract T community resolutions, after which training and inference follow an MLP-style pipeline on features of dimension $D + Td_c$. This yields propagation-free training and adjacency-free inference, with costs scaling linearly in the number of retained resolutions T .

3.1 Rationale and Neighborhood Based Extensions

ATLAS captures graph topology by encoding community membership at multiple resolutions, creating piecewise-constant structural

signals. Coarse partitions with large communities capture slowly varying mesoscale patterns in the network, while finer partitions introduce more boundaries and localized variation—similar to how graph wavelets decompose signals across multiple scales. By concatenating community features from different resolutions, ATLAS builds an explicit multi-scale topology feature bank that complements the original node attributes X . **This multi-resolution representation enables the model to distinguish between nodes even when they belong to the same community**, providing richer structural information for downstream prediction tasks.

Multi-resolution community embeddings effectively capture multi-scale network structure, but they have an important limitation. Community detection produces hard partitions with boundaries that can be unstable due to heuristic optimization. When these boundaries are noisy, one-hot community indicators impose a sharp structural prior that may mislead predictions for nodes near community interfaces. To address this, we complement the piecewise-constant community signals with boundary-free local context through **two optional neighborhood-based augmentations**.

First, **ATLAS-NF** performs 1-hop neighbor feature aggregation, incorporating fine-grained attribute information from each node’s immediate neighborhood. Second, **ATLAS-LPF** applies label-propagation-style diffusion to training labels, generating soft neighborhood class priors that vary smoothly across edges rather than changing abruptly at partition boundaries. Both augmentations are concatenated with Z_{ATLAS} , enabling the downstream MLP to adaptively weight local smoothness assumptions—upweighting them when beneficial and downweighting them when community structure provides stronger signals.

$$\text{ATLAS-NF: } X_{\text{NF}} = AX, \quad Z_{\text{ATLAS-NF}} = [Z_{\text{ATLAS}} \parallel X_{\text{NF}}].$$

$$\text{ATLAS-LPF: } \tilde{A} = \text{RowNorm}(A) = D^{-1}A, \quad D = \text{diag}(A1_n).$$

$$Y^{(0)} = (m_{\text{tr}} 1_C^T) \odot Y \equiv \text{diag}(m_{\text{tr}})Y,$$

$$Y^{(h)} = \tilde{A} Y^{(h-1)}, \quad h = 1, \dots, H, \quad (7)$$

$$Y_{\text{LPF}} = \big\|_{h=1}^H Y^{(h)} \in \mathbb{R}^{n \times (HC)},$$

$$Z_{\text{ATLAS-LPF}} = [Z_{\text{ATLAS}} \parallel Y_{\text{LPF}}].$$

$$Z_{\text{ATLAS-NF-LPF}} = [Z_{\text{ATLAS}} \parallel X_{\text{NF}} \parallel Y_{\text{LPF}}].$$

4 Empirical Evaluation

In this section, we provide the empirical results comparing ATLAS with other graph learning methods. Our experiments focus on answering the following *research questions*:

Q1. Does ATLAS maintain accuracy across graphs with diverse structural biases?

Q2. Can ATLAS scale to large graphs without sacrificing performance?

Structural Bias. We define *structural bias* as the degree to which community structure remains informative for prediction as partitions are refined to finer resolutions. To measure this, we vary the minimum modularity threshold Q_{\min} in the adaptive search. Lower values of Q_{\min} retain more (and finer) community resolutions. Graphs exhibit *high structural bias* when refinement improves performance, *low structural bias* when improvements plateau, and *negative structural bias* when refinement degrades performance. The definitions are further formalized in Section 5.

Table 1: Eight-benchmark comparison across homophily regimes. Rightmost column reports the average rank across the eight datasets (lower is better). Cells highlighted in yellow indicate the best score for each dataset (and best Avg. Rank); blue indicates the second-best.

Model	High structural bias		Low structural bias				Negative structural bias		Overall ↓
	Cora $h_e = 0.810$	Tolokers $h_e = 0.595$	Chameleon (Filt.) $h_e = 0.236$	Amazon-Ratings $h_e = 0.380$	Questions $h_e = 0.84$	Squirrel (Filt.) $h_e = 0.207$	Actor $h_e = 0.216$	Roman-Empire $h_e = 0.047$	
MLP	75.44 \pm 1.97	72.97 \pm 0.90	36.00 \pm 4.69	39.83 \pm 0.48	71.87 \pm 0.70	35.65 \pm 2.38	38.48 \pm 0.93	66.22 \pm 0.53	14.75
GCN	87.01 \pm 1.04	74.93 \pm 1.32	37.11 \pm 3.04	42.78 \pm 0.14	76.09 \pm 1.27	32.70 \pm 1.73	28.49 \pm 0.91	45.68 \pm 0.38	16.25
SAGE	87.50 \pm 0.87	80.95 \pm 0.92	38.83 \pm 4.26	44.67 \pm 0.51	76.44 \pm 0.62	33.32 \pm 1.75	34.08 \pm 1.07	76.21 \pm 0.65	12.13
GAT	87.74 \pm 0.88	75.31 \pm 1.35	37.18 \pm 3.44	43.25 \pm 0.85	77.43 \pm 1.20	32.61 \pm 2.06	29.11 \pm 1.23	47.16 \pm 0.66	14.50
H2GCN	87.52 \pm 0.61	73.35 \pm 1.01	26.75 \pm 3.64	36.47 \pm 0.23	63.59 \pm 1.46	35.10 \pm 1.15	38.85 \pm 1.17	60.11 \pm 0.52	15.00
LinkX	82.62 \pm 1.44	81.15 \pm 1.23	42.34 \pm 4.13	52.66 \pm 0.64	71.96 \pm 2.07	40.10 \pm 2.21	35.64 \pm 1.36	56.15 \pm 0.93	10.25
GPR-GNN	79.51 \pm 0.36	72.94 \pm 0.97	39.93 \pm 3.30	44.88 \pm 0.34	55.48 \pm 0.91	38.95 \pm 1.99	39.30 \pm 0.27	64.85 \pm 0.27	13.25
FSGNN	87.51 \pm 1.21	82.76 \pm 0.61	40.61 \pm 2.97	52.74 \pm 0.83	78.86 \pm 0.92	35.92 \pm 1.32	37.65 \pm 0.79	79.92 \pm 0.56	6.75
GloGNN	88.31 \pm 1.13	73.39 \pm 1.17	25.90 \pm 3.58	36.89 \pm 0.14	65.74 \pm 1.19	35.11 \pm 1.24	37.70 \pm 1.40	59.63 \pm 0.69	15.00
FAGCN	88.85 \pm 1.36	77.75 \pm 1.05	41.90 \pm 2.72	44.12 \pm 0.30	77.24 \pm 1.26	41.08 \pm 2.27	31.59 \pm 1.37	65.22 \pm 0.56	9.13
GBK-GNN	87.09 \pm 1.52	81.01 \pm 0.67	39.61 \pm 2.60	45.98 \pm 0.71	74.47 \pm 0.86	35.15 \pm 1.65	38.47 \pm 1.53	74.57 \pm 0.47	10.38
JacobiConv	89.61 \pm 0.96	68.66 \pm 0.65	39.00 \pm 4.20	43.55 \pm 0.48	73.88 \pm 1.16	29.71 \pm 1.66	41.17 \pm 0.64	71.14 \pm 0.42	11.50
ACM-GCN	87.91 \pm 0.95	74.95 \pm 1.16	42.73 \pm 3.59	52.49 \pm 0.24	62.91 \pm 2.10	39.79 \pm 2.15	36.12 \pm 1.09	71.89 \pm 0.61	9.75
OrderedGNN	88.37 \pm 0.75	75.60 \pm 1.36	41.51 \pm 4.15	51.15 \pm 0.46	75.09 \pm 1.04	36.94 \pm 2.94	37.99 \pm 1.01	82.88 \pm 0.71	8.31
M2M-GNN	88.12 \pm 1.02	80.85 \pm 0.08	41.73 \pm 3.08	51.58 \pm 0.55	71.27 \pm 1.41	37.38 \pm 1.14	36.72 \pm 1.60	84.17 \pm 0.49	9.13
CMGNN	85.76 \pm 1.09	76.38 \pm 2.42	42.15 \pm 4.84	52.57 \pm 0.82	56.17 \pm 1.09	40.25 \pm 1.63	36.82 \pm 0.78	84.42 \pm 1.66	9.13
ATLAS	88.37 \pm 0.63	82.19 \pm 0.73	42.87 \pm 3.55	53.17 \pm 0.81	73.26 \pm 0.83	41.24 \pm 1.49	38.48 \pm 0.93	66.22 \pm 0.53	5.44
ATLAS-NF	89.08 \pm 0.44	82.88 \pm 0.78	40.02 \pm 2.79	52.30 \pm 0.64	78.17 \pm 1.12	38.13 \pm 1.16	34.26 \pm 0.97	78.10 \pm 0.59	6.88
ATLAS-LPF	88.46 \pm 0.49	82.30 \pm 0.76	42.69 \pm 4.07	52.81 \pm 0.37	74.13 \pm 0.92	40.52 \pm 2.10	38.44 \pm 1.10	70.22 \pm 0.37	5.63
ATLAS-LPF-NF	89.20 \pm 0.39	82.65 \pm 0.92	40.23 \pm 3.78	51.91 \pm 0.46	77.35 \pm 0.83	38.33 \pm 1.53	34.72 \pm 1.53	79.04 \pm 0.72	6.88
ATLAS-MLP	+12.93	+9.22	+6.87	+13.34	+1.39	+5.59	+0.00	+0.00	—
ATLAS-GCN	+1.36	+7.26	+5.76	+10.39	-2.83	+8.54	+9.99	+20.54	—

Datasets. We evaluate on 13 benchmarks spanning medium-size and million-node graphs, following standard preprocessing and evaluation protocols from prior work. We report ROC-AUC for the binary datasets (Tolokers and Questions) and Accuracy for the remaining medium datasets; for large graphs we follow the standard metric used in prior work (micro-F1 for Flickr/Reddit/Yelp/Amazon-Products and Accuracy for ogbn-products). Complete statistics and splits are given in Appendix Tables 5 and 6. Results are averaged over 10 runs (mean \pm std).

Large-scale graphs. We use Flickr, Reddit, Yelp, Amazon-Products, and ogbn-products. We adopt the standard preprocessing and splits released with GraphSAINT for Flickr/Yelp/Amazon-Products, the GraphSAGE preprocessing for Reddit, and the official OGB split for ogbn-products [11, 13, 44].

Homophilous and heterophilous graphs. We include Cora, Actor, Questions, Chameleon-Filtered, Squirrel-Filtered, Amazon-Ratings, Tolokers, and Roman-Empire. For the filtered Wikipedia datasets (Chameleon-Filtered and Squirrel-Filtered), Roman-Empire, Amazon-Ratings, Tolokers, and Questions, we use the settings and splits of Platonov et al. [28]. For Cora and Actor, we follow 60/20/20 split.

Baselines. We organize baseline methods by their underlying modeling regime and align them with our research questions.

Q1 (medium graphs spanning homophily/heterophily). *Homophilic models* include classical message-passing GNNs designed under the homophily assumption: GCN [18], GraphSAGE [11], and GAT [35]. *Heterophily-oriented models* explicitly address feature-label or structural heterophily through multi-hop aggregation, decoupled modeling, spectral filtering, or heterophily-aware propagation: H₂GCN [47], LinkX [21], GPR-GNN [8], FSGNN [24], GloGNN [19], FAGCN [3], GBK-GNN [9], JacobiConv [36], ACM-GCN [22], OrderedGNN [31], M2M-GNN [20], and CMGNN [45].

Q2 (scalability). We evaluate scalability using two classes of efficient GNNs. **Precomputation-based** methods (also called decoupled methods) improve efficiency by separating graph propagation from learning. These methods precompute multi-hop or diffused node features using fixed graph operators, then train a lightweight predictor on these features using standard i.i.d. mini-batching. This avoids costly neighborhood expansion during training. Examples include SGC [37], SIGN [29], SAGN [33], and GMLP [7]. **Sampling-based** methods reduce computation by training on sampled neighborhoods or subgraphs including GraphSAGE [11], ClusterGCN [6], GraphSAINT [44], LABOR [2], and GRAPES [41].

We use an L -layer MLP with hidden width d_{hid} and dropout rate p . Each of the first $L-1$ layers applies *Linear (with bias) \rightarrow Layer-Norm \rightarrow GELU \rightarrow Dropout*. The final layer is a *Linear* classifier to C classes.

4.1 Q1: Accuracy Across Structural-Bias Regimes

Table 1 presents results across eight benchmarks spanning high, low, and negative structural-bias regimes (Sec. 5), with edge homophily (h_e) for context. The ATLAS variants serve as a diagnostic toolbox: MLP isolates attribute signal (X only), ATLAS adds multi-resolution community features, ATLAS-NF incorporates 1-hop neighbor-aggregated attributes, and ATLAS-LPF adds degree-normalized label priors (ATLAS-LPF-NF combines both).

The results reveal regime-dependent patterns; (i) high-bias datasets show gains primarily from community features, improving over both MLP and GCN; (ii) low-bias datasets challenge GNNs due to subtle structural signals. ATLAS remains competitive by capturing coarse structure; and (iii) negative-bias datasets offer even less label-relevant structural information, so performance depends mainly on features. ATLAS matches MLP, while additional gains

Table 2: Large-graph performance. We report micro-F1 (%) on Flickr/Reddit/Yelp/AmazonProducts and Accuracy (%) on ogbn-products. Cells highlighted in yellow indicate the best score for each dataset (and best Avg. Rank); blue indicates the second-best.

Method	High structural bias		Low structural bias		Negative structural bias		Overall Avg. Rank ↓
	Reddit $h_c=0.756$	ogbn-products $h_c=0.808$	Flickr $h_c=0.319$	Yelp $h_c=0.809$	AmazonProducts $h_c=0.116$		
MLP	74.35±0.16	61.06±0.08	47.17±0.11	65.46±0.11	82.04±0.02	9.40	
GCN	93.30±0.01	75.64±0.21	49.20±0.30	37.80±0.10	28.10±0.50	12.80	
GraphSAGE	95.30±0.10	80.61±0.16	50.10±1.30	63.40±0.60	75.80±0.20	6.80	
ClusterGCN	95.40±0.10	78.62±0.61	48.10±0.50	60.90±0.50	75.90±0.80	8.60	
GraphSAINT	96.60±0.10	75.36±0.34	51.10±0.10	65.30±0.30	81.50±0.10	5.40	
LABOR	96.23±0.05	78.59±0.34	51.67±0.27	61.57±0.67	68.25±0.10	6.60	
GRAPES	94.30±0.06	71.45±0.20	49.54±0.67	44.57±0.88	62.01±0.06	12.00	
SGC	93.51±0.04	67.48±0.11	50.35±0.05	23.56±0.02	22.62±0.28	13.20	
SIGN	95.95±0.02	80.52±0.16	51.60±0.11	57.98±0.12	74.24±0.02	6.80	
SAGN	96.48±0.03	81.21±0.07	50.07±0.11	61.55±0.40	76.82±1.15	5.60	
GAMLP	96.62±0.03	83.76±0.19	52.58±0.12	57.84±1.54	75.99±0.26	4.40	
ATLAS	95.74±0.04	79.98±0.14	51.56±0.14	65.46±0.11	82.04±0.02	4.40	
ATLAS-NF	94.10±0.07	75.07±0.30	52.72±0.11	57.40±0.21	77.83±0.10	8.20	
ATLAS-LPF	96.65±0.04	80.34 ± 0.33	51.77±0.16	60.20±1.34	56.64±0.28	6.00	
ATLAS-LPF-NF	94.47±0.10	75.14±0.30	52.80±0.17	51.92±2.07	53.70±0.48	9.40	
ATLAS-MLP	+21.39	+18.92	+4.39	+0.00	+0.00	—	
ATLAS-GCN	+2.44	+4.34	+2.36	+27.66	+53.94	—	

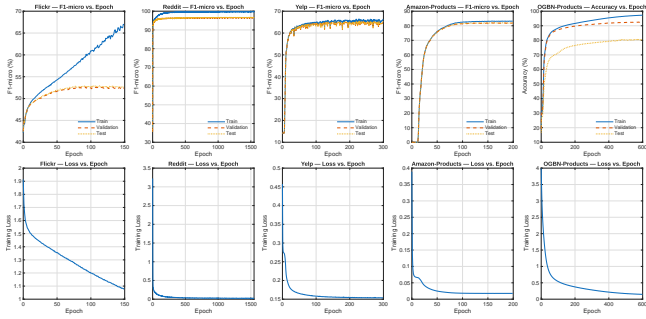


Figure 4: The convergence landscape of ATLAS.

can come from neighborhood features and label priors (e.g., Roman-Empire).

Comparative Performance. ATLAS achieves the lowest average rank (5.44) and dominates high and low structural bias categories. It excels on challenging low-bias datasets at 52.64% accuracy, beating FSGNN by +0.61%. ATLAS-NF leads high-bias datasets at 85.98% (+0.84% vs. FSGNN). Though CMGNN outperforms ATLAS on negative-bias datasets but this affects only the Roman-Empire.

ATLAS thus provides both strong performance and a principled framework for dissecting GNN contributions that reveals how community structure, local features, and attributes each contribute to prediction accuracy.

4.2 Q2: Efficiency and Scalability on Large Graphs

Table 2 shows that ATLAS remains competitive at million-node scale while preserving propagation-free inference. Predictions are produced by an MLP over $[X||E]$, optionally augmented with *pre-computed* local signals (NF/LPF).

Table 3: Complexity comparison. $N = \# \text{nodes}$, $\|A\|_0 = \# \text{edges}$, $D = \text{feature dim}$, $L = \# \text{message-passing layers}$, $L_{ff} = \# \text{feed-forward layers}$, $b = \text{batch size}$, $r = \text{sampled neighbors (or filter size)}$, $K = \# \text{precomputed hop propagations}$, $k = \# \text{subgraph samples (GraphSAINT)}$, $T = \# \text{resolutions}$, $d_c = \text{community-embedding dim}$.

Method	Pre	Train/epoch	Mem
GCN (full)	—	$O(L(\ A\ _0 D + ND^2))$	$O(L(ND + D^2))$
ClusterGCN	$O(\ A\ _0)$	$O(L(\ A\ _0 D + ND^2))$	$O(L(BD + D^2))$
GraphSAINT	$O(kN)$	$O(L(\ A\ _0 D + ND^2))$	$O(LBD)$
SAGN	$O(K\ A\ _0 D)$	$O(L_{ff}NK^2D^2)$	$O(bL_{ff}KD)$
GAMLP	$O(K\ A\ _0 D)$	$O(L_{ff}NK^2D^2)$	$O(bL_{ff}KD)$
ATLAS	$O(T\ A\ _0)$	$O(L_{ff}N(D + Td_c)^2)$	$O(bL_{ff}(D + Td_c))$

ATLAS represents the superior choice for graph neural network applications through its intelligent, modular architecture that adaptively leverages different graph signals based on structural characteristics. Its community features (E) provide a robust multi-scale foundation, achieving strong baseline performance without message passing (95.74% on Reddit, 79.98% on ogbn-products), while its Label Propagation Features (LPF) and Node Features (NF) components activate selectively when beneficial. On negative structural bias datasets where graph topology misleads, ATLAS achieves optimal performance (65.46% on Yelp, 82.04% on AmazonProducts) by intelligently avoiding harmful propagation, outperforming GAMLP by 7-8% and improving up to 53.94% over traditional GCN.

Conversely, on label-aligned graphs, ATLAS-LPF captures beneficial neighborhood information, while ATLAS-NF and ATLAS-LPF-NF excel when local attribute aggregation adds complementary context (achieving best-in-class 52.80% on Flickr). This flexibility, combined with ATLAS’s tied-best 4.40 average rank and lower performance variance across dataset types, makes it the safer choice for real-world deployments where structural bias is unknown.

Convergence. ATLAS converges rapidly and stably across large graphs. Training loss decreases smoothly, and validation performance plateaus early with a small train-validation gap. The curves show no late-epoch degradation and remain stable after convergence (see Fig. 4).

Efficiency. Table 3 shows that ATLAS adds a T -resolution community search as a one-time preprocessing step with cost $O(T\|A\|_0)$, after which training is MLP-like and inference is adjacency-free on features of dimension $D + Td_c$. T is a controllable hyperparameter. Increasing Q_{\min} retains fewer (coarser) resolutions and substantially reduces preprocessing time (see Appendix Table 4 for the timings).

ATLAS delivers consistent excellence across all graph types, matching theoretical optimums when structure is harmful and competitive peak performance when structure helps.

5 Structural Bias Effects on Multi-Scale Refinement

We quantify community refinement through the minimum modularity threshold Q_{\min} . Large Q_{\min} retains only coarse communities, while lowering Q_{\min} progressively incorporates medium and

fine-grained communities for multi-scale representation. We define *structural bias* as how effectively a graph’s community structure supports classification. We identify three distinct classes.

- **High structural bias** (e.g., Cora, Tolokers): Communities strongly align with labels. Coarse communities at large Q_{\min} already carry substantial signal, and incorporating finer communities steadily improves performance until saturation (Figure 6, top/bottom left). Both GCN and ATLAS significantly outperform MLP.
- **Low structural bias** (e.g., Amazon-Ratings, Chameleon-Filtered, Flickr, Squirrel-Filtered): Weak label-community alignment limits structural signal. Coarse communities capture most available information, and adding finer resolutions yields only modest gains. ATLAS moderately improves over MLP while GCN shows minimal or no improvement (Figure 6, top/bottom center).
- **Negative structural bias** (e.g., Actor, Roman-Empire): Community structure actively misleads classification. Finer communities inject noise, causing performance to deteriorate as Q_{\min} decreases (Figure 6, top/bottom right).

Experimental Validation of Theory. Figure 5 demonstrates how community refinement behavior aligns with our NMI theory (Section 2). As resolution parameter γ increases, communities become progressively refined, and consistent with Lemmas 1-2, both mutual information $I(L; C)$ and entropy $H(C)$ grow monotonically across all datasets. Theorem 1 shows why NMI exhibits distinct patterns across structural-bias regimes. On high-bias graphs, NMI forms an interior peak where optimal label-community alignment occurs; on low-bias graphs, NMI remains low and relatively flat because gains in $I(L; C)$ fail to outpace entropy growth, indicating weak structural signal; on negative-bias graphs, NMI rises slowly from near-zero and plateaus at modest levels, reflecting fundamental misalignment between community structure and labels.

Illustrative Example. On Cora (Fig. 6 top left), each Q_{\min} threshold selects resolutions whose modularity satisfies $Q(\gamma) \geq Q_{\min}$. Detailed breakdown of the modularity, communities and accuracy is given in Table 7 in the Appendix.

At $Q_{\min} \in \{1.0, 0.9\}$, no resolutions qualify and ATLAS defaults to feature-only MLP (76.61%). At $Q_{\min} = 0.8$, adding two resolutions raises accuracy to 79.93%; subsequent decreases to 0.7 and 0.6 incorporate medium and fine resolutions, boosting performance to 83.66% and 86.50% respectively. The ATLAS curve overtakes GCN as additional resolutions are included, peaking at 88.10% when $Q_{\min} = 0.1$. Further reduction to 0.0 adds overly fragmented communities that act as noise, causing slight degradation.

6 Ablation Study

Effect of Modularity Gap and Resolution on Performance. The modularity gap fundamentally shapes refinement behavior by determining how many Louvain resolutions are selected and their respective predictive value. Small average gaps retain many closely-spaced resolutions, while large gaps leave only a few widely-separated ones, creating a trade-off between redundant partitions and overly-coarse structure.

On **high structural-bias graphs** (Figure 7(a)) all three datasets (Cora, Tolokers, and Reddit2) exhibit a clear inverted-U relationship between modularity gap and accuracy, though with different baseline performance levels.

Reddit2 maintains consistently high accuracy (94-96%) with minimal variation across gap values, showing only a slight decline at very large gaps. Cora demonstrates the clearest inverted-U pattern: starting at approximately 84% accuracy with very small gaps ($gap < 0.01$), performance rises steadily as the gap increases, reaching a peak of approximately 88% around $gap \approx 0.05 - 0.07$, before declining back to roughly 85-86% at larger gaps ($gap > 0.12$). Tolokers shows similar behavior but with lower overall accuracy, starting near 79-80%, peaking at approximately 83% around $gap \approx 0.08$, then declining to around 81-82% at large gaps.

When the gap is very small, ATLAS retains many nearly-redundant partitions whose overlapping community features inject noise. As the gap reaches an optimal moderate range, the selected resolutions capture distinct granularities that align well with labels, strengthening mutual information and improving accuracy. When the gap becomes too large, only a handful of coarse resolutions remain, providing insufficient detail to exploit the available structural signal.

For **low structural-bias graphs** (Figure 7(b)), the behavior differs markedly. Amazon-Rating maintains the most stable performance, staying relatively flat between 53-54% across all gap values. Flickr shows slight fluctuation around 49-51% with a modest peak near $gap \approx 0.03 - 0.05$ before stabilizing. Chameleon exhibits the most variability, fluctuating between approximately 39-42%. Since community structure in these graphs carries minimal label information, varying the modularity gap primarily changes how many resolutions are retained without making them substantially more predictive. Consequently, adding community features yields only modest gains over feature-only baselines.

Figure 7(c) reveals **the mechanism underlying this behavior** by plotting the relationship between modularity gap and the number of resolutions retained for Cora. The curve demonstrates a steep exponential decay. At very small gaps ($gap \approx 0.01$), the algorithm retains approximately 36 resolutions, many of which are nearly identical and thus provide redundant features that limit accuracy to around 84% (see panel (a)). As the gap increases to moderate values ($gap \approx 0.05 - 0.07$), the resolution count drops to approximately 14-16, representing a compact set that captures meaningful structural granularities. This corresponds to the peak accuracy of 88% in panel (a).

Beyond $gap \approx 0.08$, the decay continues more gradually, with resolution counts falling to approximately 9-11 at $gap \approx 0.10 - 0.12$, which still captures useful structure but with diminishing returns. At very large gaps ($gap > 0.15$), fewer than 5 resolutions remain, too coarse to capture the label-relevant structure, corresponding to the accuracy decline seen in panel (a). This resolution count trajectory directly explains the inverted-U accuracy pattern in high-bias dataset. **Optimal performance emerges where the gap strikes a balance between retaining sufficient structural information (enough resolutions) and avoiding feature redundancy (not too many overlapping resolutions).**

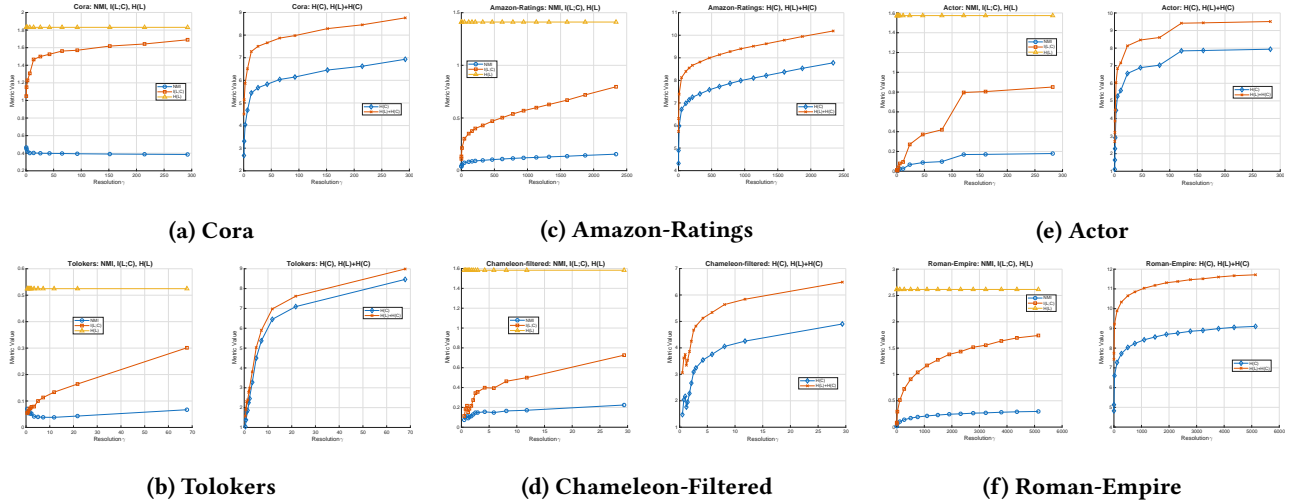


Figure 5: NMI, mutual information, and entropy dynamics across resolutions. High structural bias datasets (Cora and Tolokers, left); low structural bias datasets (Amazon and Chameleon-Filtered, middle); negative structural bias datasets (Actor and Roman-Empire, right).

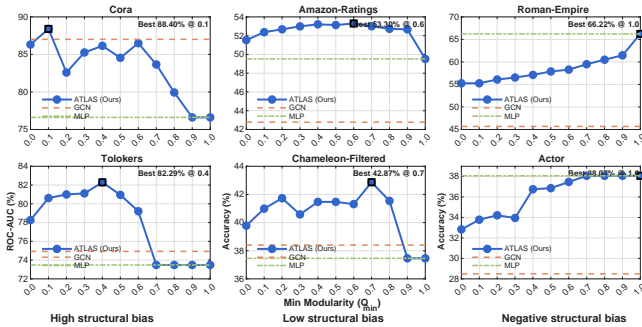


Figure 6: Effect of cumulatively adding community-derived features as the minimum modularity threshold Q_{\min} is lowered, for high structural bias graphs (left), low structural bias graphs (middle), and negative structural bias graphs (right).

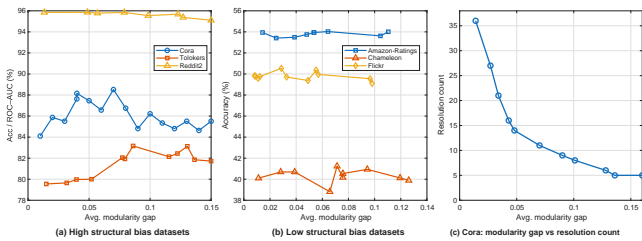


Figure 7: (a-b) Accuracy/ROC-AUC vs. average modularity gap on high- and low-structural-bias datasets. (c) Resolution count vs. modularity gap for Cora.

7 Related Work

GNNs are a core tool for learning on graphs [11, 18]. Most algorithms follow a message-passing paradigm, aggregating transformed neighbor features into topology-aware embeddings, that assumes

homophily [47]. This bias can blur informative distinctions on weakly homophilous or heterophilous graphs [27, 47].

Scaling GNNs on large graphs. Scaling GNNs on large graphs faces memory and aggregation challenges. Sampling-based methods (GraphSAGE, FastGCN, Cluster-GCN) [5, 6, 11] introduce stochasticity affecting convergence [48]. Decoupled models precompute feature diffusion and train MLPs on fixed features, enabling fast i.i.d. mini-batching (SGC, SIGN, GMLP) [7, 29, 37].

Learning on non-homophilous graphs. For non-homophilous graphs, methods preserve self-features while injecting neighborhood information (H2GCN, GloGNN) [19, 47], or reweight neighbors (GPR-GNN, FAGCN) [3, 8]. Others exploit higher-order propagation to capture heterophilic signals (MixHop, BernNet) [1, 12].

Community-aware node embeddings. Some works use community structure for prediction. Sun et al. [32] jointly infer communities and embeddings via edge reconstruction. Kamiński et al. [16] construct community-derived features showing strong performance on node tasks.

Hussain et al. [14] show GNN gains are largest when labels follow communities, linking the cluster assumption [4] with graph-task alignment analyses [39].

Community-guided rewiring. ComMa and ComFy [30] use community structure to rewire edges, improving label-community alignment and GNN accuracy. Unlike these approaches, ATLAS treats multi-resolution community assignments as MLP features, remaining propagation-free while leveraging community structure.

8 Limitations and Future Work

Limitations of the theoretical framework. Our analysis assumes *idealized* nested partitions $C' \preceq C$. In practice, community detection may yield non-nested partitions, so refinement should be viewed as a guideline. The framework measures label-community

alignment via NMI but does not model node attributes or predictors, providing no task-level accuracy guarantees. Extending to approximate refinements and connecting alignment to learning dynamics remains important future work.

Limitations of Louvain-based extraction. ATLAS runs modularity optimization at multiple resolution values requiring T separate optimizations as multilevel coarsening. This increases preprocessing cost, and modularity sensitivity to initialization which affects feature stability. Future work includes warm-starting with neighboring γ values, thereby exploring hierarchical methods for computing multiple granularities in fewer passes, and using communities for label-aware graph rewiring to amplify useful signals.

9 Conclusion

We introduced ATLAS, a propagation-free graph learning framework that injects topology through *multi-resolution community structure*. By extracting community assignments across resolutions, projecting and concatenating them with node features, and training a compact MLP, ATLAS captures multi-scale structural information, yielding an efficient training and inference pipeline for both medium and million-node graphs.

Across a diverse suite of homophilic and heterophilic benchmarks, ATLAS achieves competitive or superior accuracy relative to strong homophily-oriented GNNs, heterophily-oriented models, and scalable decoupled/sampling baselines, while maintaining stable convergence and adjacency-free inference once preprocessing is complete. Our structural-bias analysis shows that refinement systematically helps when community structure aligns with labels and can hurt when it is misaligned, providing an interpretable view of when topology is beneficial for node classification.

Use of Generative AI. We have used generative AI to polish the writing, and to check that the proofs of the theorem and lemma are correct and concise.

Reproducibility Statement. Our source code is available at <https://github.com/atlaspaper16/ATLAS>.

References

- [1] Sami Abu-El-Haija, Bryan Perozzi, Aron Kapoor, Nazanin Alipourfard, Kristina Lerman, Hravir Harutyunyan, Greg Ver Steeg, and Aram Galstyan. 2019. Mix-Hop: Higher-order graph convolutional architectures via sparsified neighborhood mixing. In *Proceedings of the 36th International Conference on Machine Learning (ICML) (Proceedings of Machine Learning Research, Vol. 97)*. PMLR, 21–29. <https://proceedings.mlr.press/v97/abu-el-haija19a.html>
- [2] Muhammed Fatih Balın and Ümit V. Çatalyürek. 2023. Layer-Neighbor Sampling – Defusing Neighborhood Explosion in GNNs. In *Advances in Neural Information Processing Systems (NeurIPS)*. arXiv:2210.13339 [cs.LG] <https://arxiv.org/abs/2210.13339>
- [3] Deyu Bo, Xiao Wang, Chuan Shi, and Huawei Shen. 2021. Beyond Low-Frequency Information in Graph Convolutional Networks. In *AAAI Conference on Artificial Intelligence (AAAI)*. 3950–3957. <https://ojs.aaai.org/index.php/AAAI/article/view/16514>
- [4] Olivier Chapelle, Bernhard Schölkopf, and Alexander Zien (Eds.). 2006. *Semi-Supervised Learning*. MIT Press.
- [5] Jie Chen, Tengfei Ma, and Cao Xiao. 2018. FastGCN: Fast Learning with Graph Convolutional Networks via Importance Sampling. In *International Conference on Learning Representations (ICLR)*. <https://openreview.net/forum?id=rytstxWAW>
- [6] Wei-Lin Chiang, Xuanqing Liu, Si Si, Yang Li, Samy Bengio, and Cho-Jui Hsieh. 2019. Cluster-GCN: An Efficient Algorithm for Training Deep and Large Graph Convolutional Networks. In *Proceedings of the 25th ACM SIGKDD International Conference on Knowledge Discovery & Data Mining (KDD)*. 257–266. doi:10.1145/3292500.3330925
- [7] Eli Chien, Xiao Pan, Jie Peng, and Olgica Milenkovic. 2022. Node Feature Reuse and Self-Ensembling for Fast Graph Neural Networks. In *Proceedings of the International Conference on Machine Learning*.
- [8] Eli Chien, Jianhao Peng, Pan Li, and Olgica Milenkovic. 2021. Adaptive Universal Generalized PageRank Graph Neural Network. In *International Conference on Learning Representations (ICLR)*. arXiv:2006.07988 [cs.LG] <https://openreview.net/forum?id=n0j7FlxrP>
- [9] Lun Du, Xiaozhou Shi, Qiang Fu, Xiaojun Ma, Hengyu Liu, Shi Han, and Dongmei Zhang. 2022. GBK-GNN: Gated Bi-Kernel Graph Neural Networks for Modeling Both Homophily and Heterophily. In *Proceedings of the ACM Web Conference (WWW '22)*. ACM, 1550–1558. doi:10.1145/3485447.3512201
- [10] Aditya Grover and Jure Leskovec. 2016. node2vec: Scalable Feature Learning for Networks. In *KDD*. doi:10.1145/2939672.2939754
- [11] William L. Hamilton, Rex Ying, and Jure Leskovec. 2017. Inductive Representation Learning on Large Graphs. In *Advances in Neural Information Processing Systems (NeurIPS)*, Vol. 30. arXiv:1706.02216 <https://papers.nips.cc/paper/6703-inductive-representation-learning-on-large-graphs>
- [12] Xinshe He, Kan Chen, Lu Sheng, Jingchang Xu, Qibin He, Jiashi Cheng, and Ping Luo. 2021. BernNet: Learning Arbitrary Graph Spectral Filters via Bernstein Approximation. In *Advances in Neural Information Processing Systems*.
- [13] Weihua Hu, Matthias Fey, Marinka Zitnik, Yuxiao Dong, Hongyu Ren, Bowei Liu, Michele Catasta, and Jure Leskovec. 2020. Open Graph Benchmark: Datasets for Machine Learning on Graphs. In *Advances in Neural Information Processing Systems (NeurIPS)*. arXiv:2005.06875 <https://proceedings.neurips.cc/paper/2020/hash/fb60d411a5c5b72b2e7d3527fc84fd0-Abstract.html>
- [14] Hussain Hussain, Tomislav Duricic, Elisabeth Lex, Denis Helic, and Roman Kern. 2021. The interplay between communities and homophily in semi-supervised classification using graph neural networks. *Applied Network Science* 6, 1 (2021), 80.
- [15] Jaykumar Kakkad, Jaspal Jannu, Kartik Sharma, Charu Aggarwal, and Sourav Medya. 2023. A Survey on Explainability of Graph Neural Networks. arXiv:2306.01958 [cs.LG] <https://arxiv.org/abs/2306.01958>
- [16] Bogumił Kamiński, Paweł Pralat, François Théberge, and Sebastian Zająć. 2024. Predicting properties of nodes via community-aware features. *Social Network Analysis and Mining* 14, 117 (2024). doi:10.1007/s13278-024-01281-2
- [17] Bhaskar Khemani. 2024. A review of graph neural networks: concepts, architectures, and applications. *Journal of Big Data* (2024). doi:10.1186/s40537-023-00876-4
- [18] Thomas N. Kipf and Max Welling. 2017. Semi-Supervised Classification with Graph Convolutional Networks. In *International Conference on Learning Representations*. <https://openreview.net/forum?id=SLU4ayYgI>
- [19] Xiaorui Li, Biao Wang, Yi Jiang, Wenjie Zhang, Lu Qin, and Ying He. 2022. Finding Global Homophily in Graph Neural Networks When Meeting Heterophily. In *International Conference on Machine Learning (ICML) (Proceedings of Machine Learning Research, Vol. 162)*. 13242–13256. <https://proceedings.mlr.press/v162/li22ad.html>
- [20] Langzhang Liang, Sunwoo Kim, Kijung Shin, Zenglin Xu, Shirui Pan, and Yuan Qi. 2024. Sign is Not a Remedy: Multiset-to-Multiset Message Passing for Learning on Heterophilic Graphs. In *Proceedings of the 41st International Conference on Machine Learning (ICML 2024) (Proceedings of Machine Learning Research, Vol. 235)*. PMLR, 29621–29643. <https://proceedings.mlr.press/v235/liang24c.html>
- [21] Derek Lim, Felix Hohne, Xiyu Li, Sijia Linda Huang, Vaishnavi Gupta, Omkar Bhalerao, and Ser-Nam Lim. 2021. Large Scale Learning on Non-Homophilous Graphs: New Benchmarks and Strong Simple Methods. In *Advances in Neural Information Processing Systems (NeurIPS)*, Vol. 34. 30471–30483. arXiv:2110.14446 <https://proceedings.neurips.cc/paper/2021/hash/ae816a80e4c1c56caa2eb4e1819ccb2f-Abstract.html>
- [22] Sitan Luan, Chenghua Lin, Qincheng Lu, Jiaqi Zhu, Mingde Zhao, Shuyuan Zhang, Xiao-Wen Chang, and Doina Precup. 2022. Revisiting Heterophily for Graph Neural Networks. In *Advances in Neural Information Processing Systems (NeurIPS)*. arXiv:2210.07606 [cs.LG] <https://arxiv.org/abs/2210.07606>
- [23] Dongsheng Luo, Wei Cheng, Dongkuan Xu, Wenchao Yu, Bo Zong, Haifeng Chen, and Xiang Zhang. 2020. Parameterized Explainer for Graph Neural Network. In *Advances in Neural Information Processing Systems*, Vol. 33. Curran Associates, Inc., 19620–19631.
- [24] Sunil Kumar Maura, Tsuyoshi Murata, and Leman Akoglu. 2022. Simplifying Approach to Node Classification in Graph Neural Networks. *Pattern Recognition Letters* 155 (2022), 116–123. doi:10.1016/j.patrec.2021.11.018 Original preprint: arXiv:2105.07634 (FSGNN).
- [25] Hongbin Pei, Bingzhe Wei, Jie Chen, Yiming Lei, and Weinan Zhang. 2020. Geom-GCN: Geometric Graph Convolutional Networks. In *International Conference on Learning Representations (ICLR)*. arXiv:2002.05287 <https://openreview.net/forum?id=S1e2agFvS>
- [26] Bryan Perozzi, Rami Al-Rfou, and Steven Skiena. 2014. DeepWalk: Online Learning of Social Representations. In *KDD*. doi:10.1145/2623330.2623732
- [27] Oleg Platonov, Denis Kuznedelev, Artem Babenko, and Liudmila Prokhorenkova. 2023. Characterizing Graph Datasets for Node Classification: Homophily-Heterophily Dichotomy and Beyond. *arXiv preprint*

arXiv:2209.06177 (2023).

[28] Oleg Platonov, Denis Kuznedelev, Michael Diskin, Artem Babenko, and Liudmila Prokorenkova. 2023. A Critical Look at the Evaluation of GNNs under Heterophily: Are We Really Making Progress? *arXiv preprint arXiv:2302.11640* (2023). <https://arxiv.org/abs/2302.11640>

[29] Emanuele Rossi, Benjamin P. Chamberlain, Fabrizio Frasca, Roberto Barbero, Davide Eynard, Michael Bronstein, and Pietro Liò. 2020. SIGN: Scalable Inception Graph Neural Networks. In *Advances in Neural Information Processing Systems*.

[30] Celia Rubio-Madrigal, Adarsh Jamadandi, and Rebekka Burkholz. 2025. GNNs Getting ComFy: Community and Feature Similarity Guided Rewiring. In *International Conference on Learning Representations (ICLR)*. <https://arxiv.org/abs/2502.04891>

[31] Yunchong Song, Chenghu Zhou, Xinbing Wang, and Zhouhan Lin. 2023. Ordered GNN: Ordering Message Passing to Deal with Heterophily and Over-smoothing. In *The Eleventh International Conference on Learning Representations (ICLR)*. <https://openreview.net/forum?id=wKPMpBHSnT6>

[32] Fan-Yun Sun, Meng Qu, Jordan Hoffmann, Chin-Wei Huang, and Jian Tang. 2019. vGraph: A Generative Model for Joint Community Detection and Node Representation Learning. In *NeurIPS*. <https://papers.nips.cc/paper/8342-vgraph-a-generative-model-for-joint-community-detection-and-node-representation-learning.pdf>

[33] Ke Sun, Zimo Zhou, Zhiqiang Zhang, Bin Cui, Yang Yang, and Liang He. 2021. Scalable and Adaptive Graph Neural Networks with Self-Label-Enhanced training. *arXiv preprint arXiv:2104.09376* (2021).

[34] Jian Tang, Meng Qu, Mingzhe Wang, Ming Zhang, Jun Yan, and Qiaozhu Mei. 2015. LINE: Large-scale Information Network Embedding. In *WWW*. doi:10.1145/2736277.2741093

[35] Petar Veličković, Guillem Cucurull, Arantxa Casanova, Adriana Romero, Pietro Liò, and Yoshua Bengio. 2018. Graph Attention Networks. In *International Conference on Learning Representations (ICLR)*. arXiv:1710.10903 <https://openreview.net/forum?id=rJXMpikCZ>

[36] Xiyuan Wang and Muhan Zhang. 2022. How Powerful are Spectral Graph Neural Networks? In *International Conference on Machine Learning (ICML) (Proceedings of Machine Learning Research, Vol. 162)*. 23341–23362. <https://arxiv.org/abs/2205.11172> Introduces JacobiConv.

[37] Felix Wu, Amauri Souza, Tianyi Zhang, Christopher Fifty, Tao Yu, and Kilian Q. Weinberger. 2019. Simplifying Graph Convolutional Networks. In *Proceedings of the International Conference on Machine Learning*.

[38] Zonghan Wu, Shirui Pan, Fengwen Chen, Guodong Long, Chengqi Zhang, and Philip S. Yu. 2019. A Comprehensive Survey on Graph Neural Networks. *arXiv:1901.00596* (2019). <https://arxiv.org/abs/1901.00596>

[39] Chenxiao Yang, Qitian Wu, David Wipf, Ruoyu Sun, and Junchi Yan. 2024. How Graph Neural Networks Learn: Lessons from Training Dynamics. In *Proceedings of the 41st International Conference on Machine Learning (Proceedings of Machine Learning Research, Vol. 235)*. PMLR, 56594–56623. <https://proceedings.mlr.press/v235/yang24ae.html>

[40] Zhitao Ying, Dylan Bourgeois, Jiaxuan You, Marinka Zitnik, and Jure Leskovec. 2019. GNNExplainer: Generating Explanations for Graph Neural Networks. In *Advances in Neural Information Processing Systems*, Vol. 32. Curran Associates, Inc., 9244–9255.

[41] Taraneh Younesian, Daniel Daza, Emile van Krieken, Thivyan Thanapalasingam, and Peter Bloem. 2025. GRAPES: Learning to Sample Graphs for Scalable Graph Neural Networks. *Transactions on Machine Learning Research* (May 2025). <https://openreview.net/forum?id=QI0l842vSq>

[42] Hao Yuan, Haiyang Yu, Jie Wang, Kang Li, and Shuiwang Ji. 2021. On Explainability of Graph Neural Networks via Subgraph Explorations. In *Proceedings of the 38th International Conference on Machine Learning (Proceedings of Machine Learning Research, Vol. 139)*. Marina Meila and Tong Zhang (Eds.). PMLR, 12241–12252. <https://proceedings.mlr.press/v139/yuan21c.html>

[43] Hongkuan Zeng, Hongkuan Zhang, Jian Shi, Jiarong Ren, Yulin Ge, Shuai Lin, and Dejing Dou. 2022. A Comprehensive Study on Large-Scale Graph Training: Benchmarking and Rethinking. In *Advances in Neural Information Processing Systems*. <https://arxiv.org/abs/2210.07494>

[44] Hanqing Zeng, Hongkuan Zhou, Ajitesh Srivastava, Rajgopal Kannan, and Viktor Prasanna. 2020. GraphSAINT: Graph Sampling Based Inductive Learning Method. In *International Conference on Learning Representations (ICLR)*. <https://openreview.net/forum?id=Bje8pkHFwS>

[45] Zhiuanan Zheng, Yuanchen Bei, Zhiyao Zhou, Sheng Zhou, Yao Ma, Ming Gu, Hongjia Xu, Jiawei Chen, and Jiajun Bu. 2025. Understanding and Enhancing Message Passing on Heterophilic Graphs via Compatibility Matrix. In *Advances in Neural Information Processing Systems (NeurIPS)*. <https://openreview.net/forum?id=4AAwJAsGvb>

[46] Jie Zhou, Ganqu Cui, Zhengyan Zhang, Cheng Yang, Zhiyuan Liu, and Maosong Sun. 2021. Graph Neural Networks: A Review of Methods and Applications. *AI Open* 1 (2021), 57–81. doi:10.1016/j.aiopen.2021.01.001

[47] Jiong Zhu, Yujun Yan, Lingxiao Zhao, Mark Heimann, Leman Akoglu, and Danai Koutra. 2020. Beyond Homophily in Graph Neural Networks: Current Limitations and Effective Designs. In *Advances in Neural Information Processing Systems (NeurIPS)*. <https://proceedings.neurips.cc/paper/2020/hash/58ae23d878a47004366189884c2f8440-Abstract.html>

[48] Difan Zou, Ziniu Hu, Yewen Wang, Song Jiang, Yizhou Sun, and Quanquan Gu. 2019. Layer-dependent importance sampling for training deep and large graph convolutional networks. In *Advances in Neural Information Processing Systems*, Vol. 32. 1125–1136. <https://dl.acm.org/doi/10.5555/3454287.3455296>

A Appendix

Compute environment. All experiments were run on a server with 1× NVIDIA A40 (45 GiB) GPU, 32 vCPUs, 2× Intel Xeon Silver 4309Y @ 2.80 GHz, and 503 GiB RAM. Software stack: Python 3.10.18; PyTorch 2.4.0+cu124 (CUDA 12.4); PyTorch Geometric 2.6.1.

A.1 Definitions and Terminology for Community Detection

This subsection defines the modularity-based community detection terms that underpin our multi-resolution community extraction.

Modularity. Given a partition $C = \{C_1, \dots, C_K\}$ with node assignments $c_i \in \{1, \dots, K\}$, *modularity* measures how much denser the intra-community connections are than expected under a degree-preserving null model:

$$Q = \frac{1}{2m} \sum_{i,j} \left(A_{ij} - \frac{k_i k_j}{2m} \right) \delta(c_i, c_j), \quad (8)$$

where A_{ij} is the adjacency matrix, k_i is the degree of node i , $m = |E|$ is the number of edges, and $\delta(c_i, c_j) = 1$ if $c_i = c_j$ (else 0). Higher Q indicates stronger community structure.

Resolution parameter. Louvain introduces a *resolution* $\gamma > 0$ to control granularity by reweighting the null-model term:

$$Q(\gamma) = \frac{1}{2m} \sum_{i,j} \left(A_{ij} - \gamma \frac{k_i k_j}{2m} \right) \delta(c_i, c_j). \quad (9)$$

Smaller γ favors coarser partitions, while larger γ typically yields finer (more, smaller) communities, providing partitions at multiple granularities across γ . We denote the resulting partition and modularity by $C(\gamma)$ and $Q^{(\gamma)}$, with assignment vector $c^{(\gamma)}$.

Modularity gap. For two values $\gamma_1 < \gamma_2$ that are adjacent after sorting the set of γ values, the *modularity gap* quantifies the change in community quality:

$$\Delta Q(\gamma_1, \gamma_2) = |Q^{(\gamma_2)} - Q^{(\gamma_1)}|. \quad (10)$$

Large gaps indicate rapid structural changes between scales and motivate inserting intermediate resolutions; small gaps suggest the refinement has stabilized.

A.2 Theoretical Proofs

LEMMA. 1. Let L be labels and C a community partition. Let C' be a refinement of C , i.e., $C' \preceq C$. Then $I(L; C') \geq I(L; C)$

PROOF. Let total number of elements be n . Then based on the definitions of $I(P, Q)$ in Section 2;

$$I(L; C') = \frac{1}{n} \sum_l \sum_{c'} n_{l,c'} \log \left(\frac{n n_{l,c'}}{n_l n_{c'}} \right),$$

$$I(L; C) = \frac{1}{n} \sum_l \sum_c n_{l,c} \log \left(\frac{n n_{l,c}}{n_l n_c} \right).$$

where $n_l = \sum_{c'} n_{l,c'}$.

$$I(L; C') - I(L; C)$$

$$= \frac{1}{n} \sum_l \sum_{c'} n_{l,c'} \log \left(\frac{n n_{l,c'}}{n_l n_{c'}} \right) - \frac{1}{n} \sum_l \sum_c n_{l,c} \log \left(\frac{n n_{l,c}}{n_l n_c} \right)$$

$$= \frac{1}{n} \sum_c \sum_{c' \subseteq c} \sum_l \left[n_{l,c'} \log \left(\frac{n n_{l,c'}}{n_l n_{c'}} \right) - n_{l,c} \log \left(\frac{n n_{l,c}}{n_l n_c} \right) \right]$$

$$= \frac{1}{n} \sum_c \sum_{c' \subseteq c} \sum_l n_{l,c'} \log \left(\frac{n_{l,c'} n_c}{n_l n_{c'}} \right).$$

Since every $c' \subseteq ofc$, therefore $\frac{n_{l,c'}}{n_{c'}} \geq \frac{n_{l,c}}{n_c}$. Thus the value in the log is positive, and $I(L; C') \geq I(L; C)$ \square

LEMMA. 2. Let C a community partition. Let C' be a refinement of C , i.e., $C' \preceq C$. Then $H(C') \geq H(C)$

PROOF. Let total size n . Based on the definition in Section 2

$$H(C) = - \sum_c \frac{n_c}{n} \log \frac{n_c}{n}, \quad H(C') = - \sum_{c'} \frac{n_{c'}}{n} \log \frac{n_{c'}}{n}.$$

By grouping the c' under their parent c :

$$H(C') - H(C) = - \sum_c \sum_{c' \subseteq c} \frac{n_{c'}}{n} \log \frac{n_{c'}}{n} + \sum_c \frac{n_c}{n} \log \frac{n_c}{n}$$

$$= \frac{1}{n} \sum_c \left[- \sum_{c' \subseteq c} n_{c'} \log n_{c'} + n_c \log n_c \right].$$

Since $f(x) = -x \log x$ is a concave function and $c' \subseteq c$, therefore,

$$\sum_{c' \subseteq c} -\frac{n_{c'}}{n} \log \frac{n_{c'}}{n} \geq -\frac{n_c}{n} \log \frac{n_c}{n}.$$

Thus, $H(C') \geq H(C)$. \square

THEOREM. Let L be labels; C a community partition. Let C' be a refinement of C , i.e., $C' \preceq C$. Then $NMI(C'; L) > NMI(C; L)$ if and only if $\frac{\Delta I}{\Delta H} > \frac{NMI(C; L)}{2}$, where $\Delta I = I(C'; L) - I(C; L)$ and $\Delta H = H(C'; L) - H(C; L)$.

PROOF.

$$NMI(C; L) = \frac{2 I(C; L)}{H(C) + H(L)}.$$

$$I := I(C; L), \quad I' := I(C'; L), \quad H := H(C),$$

$$H' := H(C'), \quad H_L := H(L).$$

Also

$$\Delta I := I' - I, \quad \Delta H := H' - H.$$

Based on Lemma 1 and 2, $\Delta I \geq 0$ and $\Delta H \geq 0$. We do not consider edge case where $\Delta H = 0$. To show

$$NMI(C'; L) > NMI(C; L) \iff \frac{\Delta I}{\Delta H} > \frac{NMI(C; L)}{2}.$$

$$\text{NMI}(C'; L) > \text{NMI}(C; L) \iff \frac{2I'}{H' + H_L} > \frac{2I}{H + H_L}.$$

$$\frac{I'}{H' + H_L} > \frac{I}{H + H_L} \iff I'(H + H_L) - I(H' + H_L) > 0.$$

Expand using $I' = I + \Delta I$ and $H' = H + \Delta H$:

$$(I + \Delta I)(H + H_L) - I(H + \Delta H + H_L) > 0.$$

Simplify terms (the $I(H + H_L)$ cancel):

$$\Delta I(H + H_L) - I\Delta H > 0.$$

Thus;

$$\Delta I(H + H_L) > I\Delta H \iff \frac{\Delta I}{\Delta H} > \frac{I}{H + H_L}.$$

By definition $\text{NMI}(C; L) = \frac{2I}{H + H_L}$, so $\frac{I}{H + H_L} = \frac{\text{NMI}(C; L)}{2}$.

Therefore

$$\text{NMI}(C'; L) > \text{NMI}(C; L) \iff \frac{\Delta I}{\Delta H} > \frac{\text{NMI}(C; L)}{2}$$

□

A.3 Algorithms

Algorithm 1 Adaptive Resolution Search for Louvain

Require: graph G , minimum modularity Q_{\min} , maximum modularity gap Δ_{\max} ; $\text{gap_range} = [a, b]$
Ensure: resolution set Γ , `community_list`

```

1:  $\mathcal{C} \leftarrow \emptyset; Q \leftarrow \emptyset$ 
2: for  $\gamma \in \{0.5, 1.0\}$  do ▷ initial resolutions
3:    $(\mathcal{C}[\gamma], Q[\gamma]) \leftarrow \text{LOUVAIN}(G, \gamma)$ 
4: while true do
5:    $L \leftarrow \text{SORTEDKEYS}(Q); \gamma_{\max} \leftarrow L[-1]; \tau \leftarrow Q[\gamma_{\max}]$ 
6:   if  $\tau \leq Q_{\min}$  then
7:     break
8:    $\gamma_{\text{new}} \leftarrow \text{None}$ 
9:   for consecutive  $(\gamma_1, \gamma_2) \in L$  do
10:    if  $|Q[\gamma_2] - Q[\gamma_1]| > \Delta_{\max}$  then
11:       $\gamma_{\text{new}} \leftarrow (\gamma_1 + \gamma_2)/2$ ; break ▷ interpolate
12:    if  $\gamma_{\text{new}} = \text{None}$  then ▷ extrapolate
13:      sample  $\delta \sim \mathcal{U}[a, b]; Q^* \leftarrow \tau - \delta$ 
14:       $s \leftarrow \text{ESTIMATESLOPE}(Q \text{ vs } \gamma)$ 
15:       $\gamma_{\text{new}} \leftarrow \gamma_{\max} + \frac{Q^* - \tau}{s}$ 
16:    $(\mathcal{C}[\gamma_{\text{new}}], Q[\gamma_{\text{new}}]) \leftarrow \text{LOUVAIN}(G, \gamma_{\text{new}})$ 
17:    $\Gamma \leftarrow \{\gamma \in \text{SORTEDKEYS}(Q) : Q[\gamma] \geq Q_{\min}\}$ 
18:   community_list  $\leftarrow [\mathcal{C}[\gamma] \text{ for } \gamma \in \Gamma]$ 
19: return  $\Gamma, \text{community\_list}$ 
```

Table 4: Preprocessing (community detection), training, and inference times.

Dataset	Preprocessing Time	Per-epoch Train Time	Inference Time
Reddit	84.904 ± 2.764	0.143 ± 0.002	0.150 ± 0.005
Flickr	6.800 ± 1.741	0.241 ± 0.005	0.056 ± 0.012
Yelp	15.842 ± 0.007	2.670 ± 0.007	1.613 ± 0.016
Amazon-Products	72.270 ± 1.409	6.073 ± 0.039	3.056 ± 0.019
Ogbn-Products	391.894 ± 14.387	0.399 ± 0.0008	0.526 ± 0.0038

Algorithm 2 Community-Augmented Feature Projection for Node Classification

Require: Graph $G = (V, E)$, node features $X \in \mathbb{R}^{n \times D}$, resolution set $\Gamma = \{\gamma_1, \dots, \gamma_T\}$, projection dimension d_c
Ensure: Predicted label distribution $\hat{Y} \in \mathbb{R}^{n \times C}$

- 1: Initialize empty list of embeddings $\mathcal{E}_{\text{emb}} \leftarrow []$
- 2: **for** $\gamma \in \Gamma$ **do**
- 3: Compute community assignment $c^{(\gamma)} \in \mathbb{N}^n$
- 4: One-hot encode $c^{(\gamma)}: H^{(\gamma)} \in \{0, 1\}^{n \times k_{\gamma}}$
- 5: Project via trainable weights: $E^{(\gamma)} \leftarrow H^{(\gamma)}W^{(\gamma)}$, where $W^{(\gamma)} \in \mathbb{R}^{k_{\gamma} \times d_c}$
- 6: Append $E^{(\gamma)}$ to \mathcal{E}_{emb}
- 7: Concatenate all embeddings: $E \leftarrow \text{Concat}(\mathcal{E}_{\text{emb}}) \in \mathbb{R}^{n \times (T \cdot d_c)}$
- 8: Concatenate with node features: $Z \leftarrow [X \parallel E] \in \mathbb{R}^{n \times (D + T \cdot d_c)}$
- 9: Predict logits with MLP: $Y \leftarrow f_{\theta}(Z) \in \mathbb{R}^{n \times C}$
- 10: Apply softmax: $\hat{Y} \leftarrow \text{softmax}(Y)$
- 11: **return** \hat{Y}

A.4 Computation time on large graphs

Table 4 summarizes ATLAS’s runtime profile on million-node benchmarks by separating the one-time preprocessing cost (multi-resolution community detection) from the per-epoch training and inference costs.

A.5 NMI Analysis for datasets

A.6 Models for homophilic graphs

GCN. Applies a linear map followed by aggregation with the symmetrically normalized adjacency (after adding self-loops), corresponding to a first-order spectral/Chebyshev approximation [18].

GAT. Learns attention coefficients over neighbors via masked self-attention and aggregates them with a softmax-weighted sum, enabling data-dependent receptive fields [35].

GraphSAGE. Performs permutation-invariant neighbor aggregation (e.g., mean, max-pooling, LSTM) with fixed fan-out sampling per layer for scalable, inductive mini-batch training on large graphs [11].

A.7 Models for heterophilic graphs

H₂GCN. Separates ego and neighbor embeddings, aggregates higher-order neighborhoods, and combines intermediate representations to improve robustness under heterophily [47].

LinkX. Separately embeds node features and adjacency (structural) information with MLPs and concatenates them, capturing complementary attribute and topology signals that scale to non-homophilous graphs [21].

GPR-GNN. Learns signed polynomial (Generalized PageRank) propagation weights, adapting the filter to both homophilous and heterophilous label patterns and mitigating over-smoothing [8].

FSGNN. Applies soft selection over hop-wise aggregated features with “hop-normalization,” effectively decoupling aggregation depth from message passing for a simple, shallow baseline that performs well under heterophily [24].

GloGNN. Augments propagation with learnable correlations to global nodes (including signed coefficients), enabling long-range information flow and improved grouping on heterophilous graphs [19].

FAGCN. Uses a self-gating, frequency-adaptive mechanism to balance low- and high-frequency components during message passing, improving robustness across homophily regimes [3].

GBK-GNN. Employs bi-kernel feature transformations with a gating mechanism to integrate homophily- and heterophily-sensitive signals within a single architecture [9].

JacobiConv. Adopts an orthogonal Jacobi-polynomial spectral basis (often without nonlinearities) to learn flexible filters suited to varying graph signal densities, yielding strong performance on heterophilous data [36].

ACM-GCN. Uses high-pass filtering with adaptive channel mixing to combine low- and high-frequency components, yielding strong performance on heterophilic and mixed-regime graphs [22].

OrderedGNN. Orders multi-hop message passing with a gating mechanism to better control how information from different hop distances is mixed, aiming to handle heterophily while mitigating over-smoothing in deep propagation [31].

M2M-GNN. Uses a *multiset-to-multiset* message passing design that partitions neighbor information into multiple subsets (instead of collapsing all neighbors into a single vector), reducing harmful mixing among heterophilous neighbors and improving robustness to over-smoothing [20].

CMGNN. Builds on a heterophilous message passing view where performance is tied to a class *compatibility matrix*; CMGNN explicitly leverages and improves this compatibility structure to enhance message passing on heterophilic graphs [45].

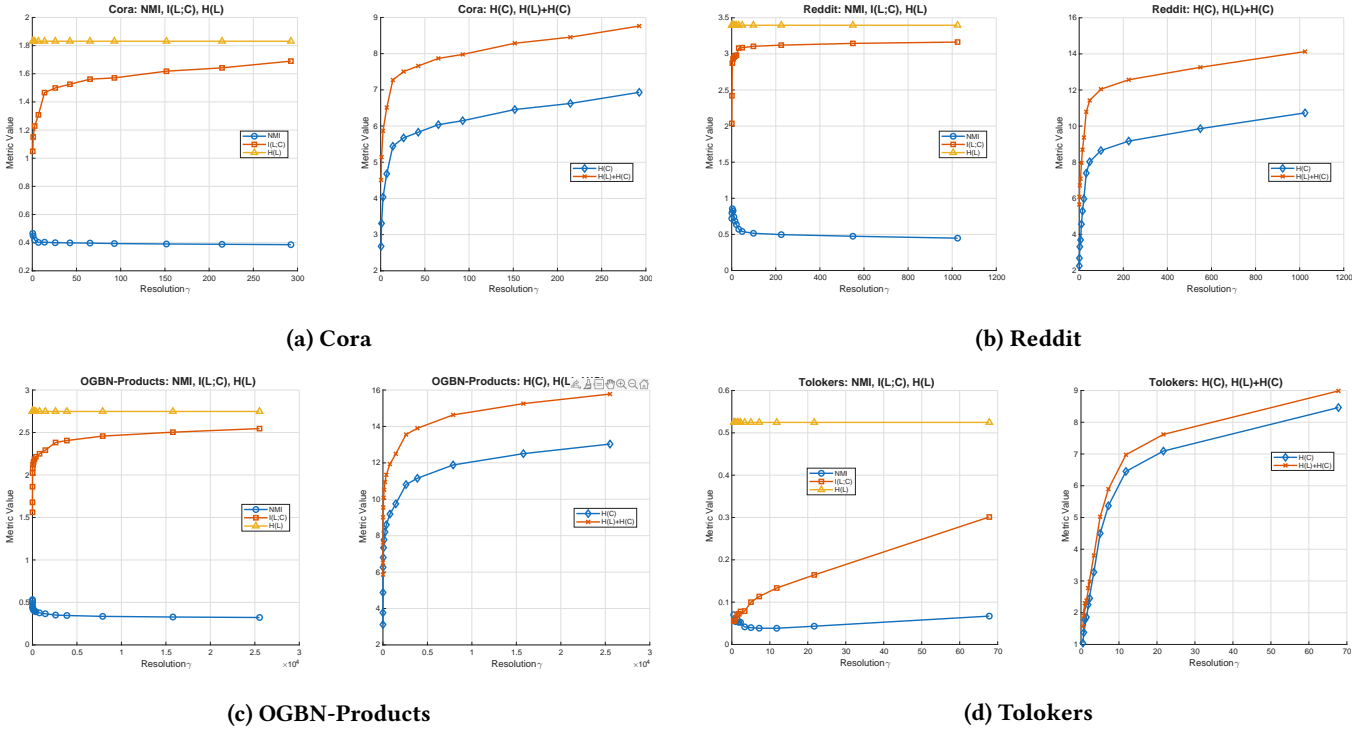


Figure 8: High structural bias datasets: (a) Cora, (b) Reddit, (c) OGBN-Products, and (d) Tolokers. Each subfigure reports how NMI , $I(L;C)$, $H(L)$, $H(C)$, and $H(L)+H(C)$ vary as the resolution parameter γ varies and yields community partitions of different granularity.

A.8 Sampling methods for scalable GNNs

GraphSAGE. Samples a fixed fan-out of neighbors per layer and learns permutation-invariant aggregators, limiting the receptive field and enabling inductive, mini-batch training on large graphs [11].

ClusterGCN. Partitions the graph and samples dense clusters as mini-batches, restricting propagation within blocks to boost edge coverage, cache locality, and memory efficiency at scale [6].

GraphSAINT. Constructs mini-batches by sampling subgraphs (node/edge-walk policies) and applies unbiased normalization to correct sampling bias, yielding strong accuracy–efficiency trade-offs on large graphs [44].

LABOR. A scalable mini-batch sampling algorithm that combines *neighbor sampling* and *layer sampling* via Poisson sampling. LABOR is designed as a drop-in replacement for fixed-fanout neighbor sampling: it correlates sampling across seed nodes to exploit overlap in their sampled neighborhoods, substantially reducing the number of sampled vertices/edges and mitigating neighborhood explosion while maintaining the per-node estimator variance properties of standard neighbor sampling [2].

GRAPES. An adaptive, layer-wise neighbor sampling method for scalable mini-batch GNN training: a sampler GNN predicts node inclusion probabilities conditioned on node features/structure and the current sampled subgraph, then selects a fixed-size set of neighbors (e.g., via a Top- k sampling trick) and is trained jointly with the

classifier using the downstream classification loss as a learning signal (via RL/GFlowNet-style estimators), improving accuracy under small sampling budgets [41].

A.9 Decoupling-based methods for scalable GNNs

SGC. Simplifies GCNs by collapsing multiple message-passing layers into a single K -step precomputation of $A^K X$, removing nonlinearities and train-time propagation. This reduces GNN training to logistic regression on pre-smoothed features, yielding strong scalability and fast inference [37].

SIGN. Precomputes multiple graph-diffused feature channels (e.g., $A^K X$ for several K), and trains an MLP on the concatenated features. This decouples feature propagation from learning entirely, enabling embarrassingly parallel preprocessing and large-batch training [29].

SAGN. Introduces a learnable gating mechanism over multiple pre-computed hop-wise representations, allowing the model to adaptively weight short- and long-range information without stacking GNN layers. This stabilizes training under heterophily and yields strong performance with shallow architectures [33].

GAMLP. Builds an ensemble over diffused feature channels using attention and prediction consistency across hops. GAMLP reuses node features efficiently and achieves high accuracy with small models, while avoiding message passing during training and inference [7].

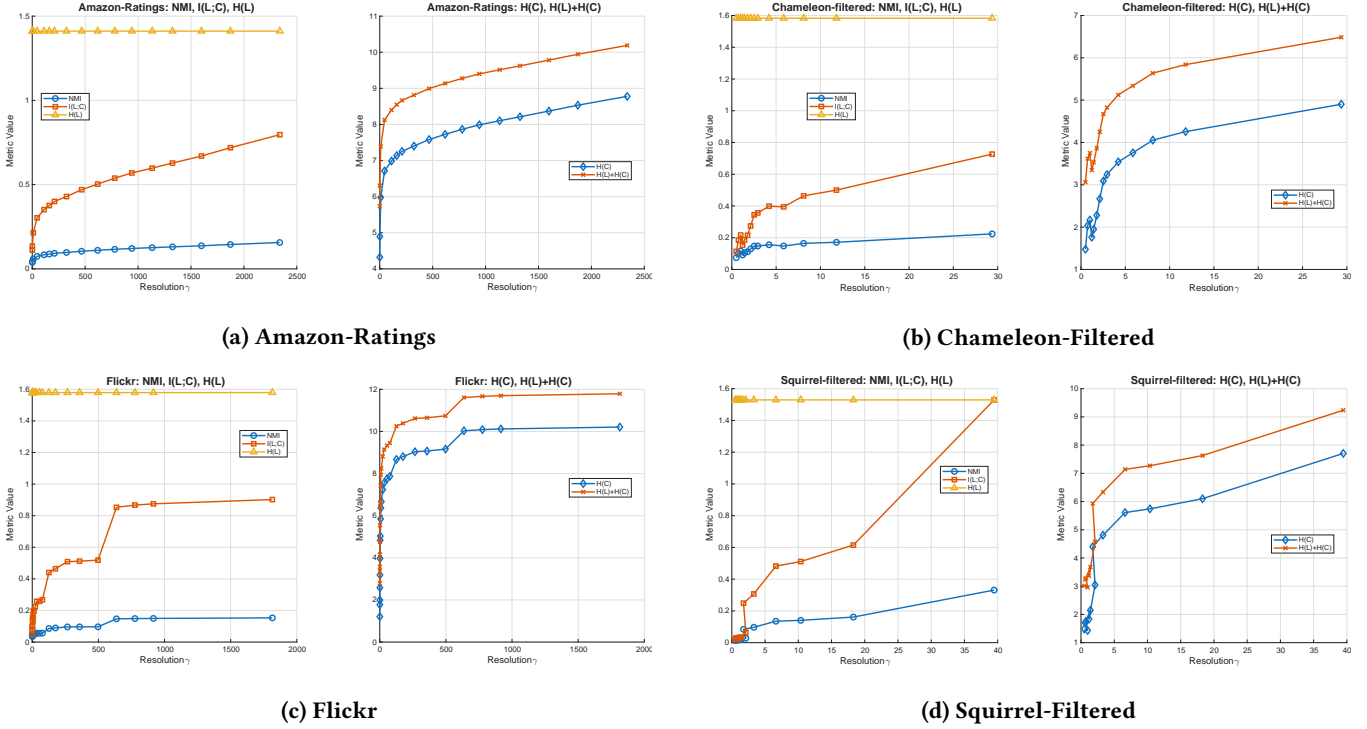


Figure 9: Low structural bias datasets: (a) Amazon-Ratings, (b) Chameleon-Filtered, and (c) Flickr (d) Squirrel-Filtered. Each subfigure illustrates how NMI , $I(L;C)$, $H(L)$, $H(C)$, and $H(L)+H(C)$ evolve as the resolution parameter γ varies and yields community partitions of different granularity.

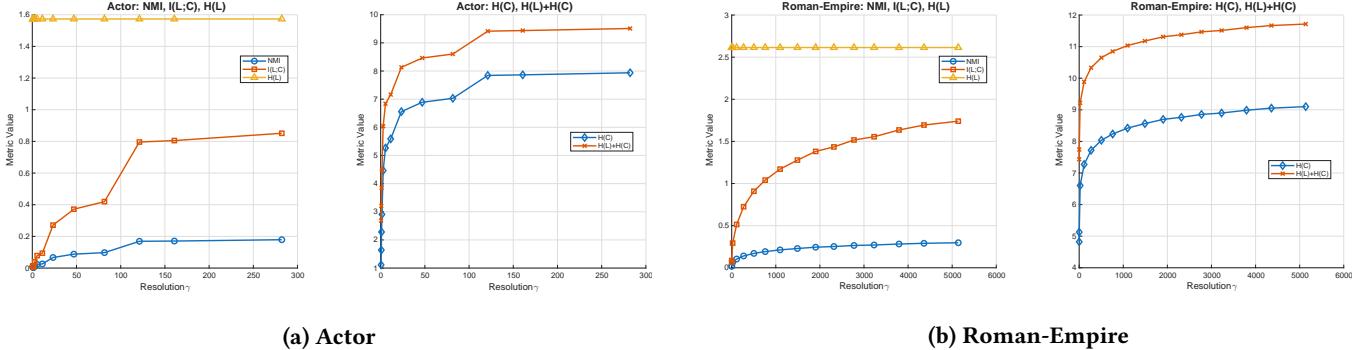


Figure 10: Negative structural bias datasets: (a) Actor and (b) Roman-Empire. Each subfigure reports how NMI , $I(L;C)$, $H(L)$, $H(C)$, and $H(L)+H(C)$ vary as the resolution parameter γ varies and yields community partitions of different granularity.

Together, these methods represent the broader “decoupling” paradigm—where propagation is performed once (or analytically) and training reduces to learning an MLP over fixed multi-hop representations—an approach systematically benchmarked and analyzed in large-scale settings by Zeng et al. [43]. ATLAS aligns with this propagation-free philosophy but differs fundamentally in how structural information is obtained: instead of precomputing $A^k X$, ATLAS extracts *multi-resolution community assignments* as topology-aware features, providing a complementary and scalable route to structural encoding.

A.10 Datasets

We evaluate on two groups of benchmarks that stress complementary regimes.

Large-scale graphs. We use Flickr, Reddit, Yelp, Amazon-Products, and ogbn-products. Flickr/Yelp/Amazon-Products come from Graph-SAINt; Reddit from GraphSAGE; ogbn-products from OGB [11, 13, 44]. Table 6 reports sizes, features, classes, and splits.

Homophilous and heterophilous graphs. We include Cora, Questions, Chameleon-Filtered, Squirrel-Filtered, Amazon-Ratings,

Tolokers, and Roman-Empire. For the filtered Wikipedia, Roman-Empire, Amazon-Ratings, Tolokers, and Questions datasets, we use the exact settings and splits of Platonov et al. [28]; Cora and Actor follow standard preprocessing [21, 25]. Table 5 lists summary stats, edge homophily h_e , and metrics.

Table 5: Dataset statistics with edge homophily h_e and evaluation metric (“Acc” for Accuracy, “ROC-AUC” for Area Under ROC).

Dataset	Nodes	Edges	Avg. Degree	Feature	Classes	Train / Val / Test	h_e	Metric
Cora	2,708	5,429	4	1,433	7 (s)	0.60 / 0.20 / 0.20 [†]	0.810	Acc
Actor	7,600	30,019	8	932	5 (s)	0.60 / 0.20 / 0.20	0.216	Acc
Questions	48,921	153,540	6	301	2 (s)	0.50 / 0.25 / 0.25	0.840	ROC-AUC
Squirrel-Filtered	2,223	65,718	59	2,089	5 (s)	0.50 / 0.25 / 0.25	0.207	Acc
Chameleon-Filtered	896	13,584	31	2,325	5 (s)	0.50 / 0.25 / 0.25	0.236	Acc
Amazon-Ratings	24,492	93,050	8	300	5 (s)	0.50 / 0.25 / 0.25	0.380	Acc
Tolokers	11,758	519,000	88	10	2 (s)	0.50 / 0.25 / 0.25	0.595	ROC-AUC
Roman-Empire	22,662	32,927	3	300	18 (s)	0.50 / 0.25 / 0.25	0.047	Acc

[†] randomly sampled to match 60/20/20 and ensures from all Louvain communities.

Table 6: Dataset statistics (“m” stands for multi-class classification, and “s” for single-class.)

Dataset	Nodes	Edges	Avg. Degree	Feature	Classes	Metric	Train / Val / Test
Flickr	89,250	899,756	10	500	7 (s)	F1-micro	0.50 / 0.25 / 0.25
Reddit	232,965	11,606,919	50	602	41 (s)	F1-micro	0.66 / 0.10 / 0.24
Yelp	716,847	6,977,410	10	300	100 (m)	F1-micro	0.75 / 0.10 / 0.15
Amazon-Products	1,598,960	132,169,734	83	200	107 (m)	F1-micro	0.85 / 0.05 / 0.10
ogbn-products	2,449,029	61,859,140	50.5	100	47 (s)	Acc	0.08 / 0.02 / 0.90

A.11 Cora: Accuracy vs. Minimum Modularity Threshold

Table 7 summarizes how relaxing the minimum modularity threshold Q_{\min} on Cora changes both the community-derived features and the resulting accuracy. Each tuple $(Q, \text{Resolution}, \text{Communities})$ corresponds to a Louvain run at resolution γ : Q is the modularity $Q(\gamma)$, and Communities is the number of communities k_{γ} whose assignments $c^{(\gamma)}$ are one-hot encoded into $H^{(\gamma)}$ and projected to a dense embedding $E^{(\gamma)}$ that is concatenated into the multi-resolution community feature matrix (Algorithm 2). For a given Q_{\min} , the row lists the cumulative set of tuples with $Q \geq Q_{\min}$: **blue tuples** are newly activated at that threshold, while **gray tuples** persist from higher thresholds. When $Q_{\min} \geq 0.9$, no tuples qualify and the model reduces to the base MLP with accuracy 76.61%. As Q_{\min} is lowered from 0.8 to 0.6, additional high-modularity, moderate-resolution community embeddings are added, and accuracy increases up to 86.50%. Further decreasing Q_{\min} admits lower-modularity, finer resolutions with many more communities, leading to small fluctuations and a peak accuracy of 88.10% at $Q_{\min} = 0.1$, where a diverse mix of coarse-to-fine community features is used. Pushing Q_{\min} to 0.0 adds one very fine tuple (768 communities), which slightly degrades performance to 86.32%, indicating that including too many extremely fine community features eventually injects noise.

Table 7: Cora: Cumulative (Q , Resolution, Communities) pairs included at each minimum modularity threshold Q_{\min} (listed in run order), with accuracy. Color coding: pairs colored in blue are newly added at that Q_{\min} ; pairs in gray were added at earlier thresholds and are carried over.

Min Modularity Q_{\min}	Pairs (Modularity, Resolution, Number of Communities)	Accuracy
1.0	—	76.61
0.9	—	76.61
0.8	(0.8526, 0.500, 90), (0.8120, 1.000, 103)	79.93
0.7	(0.8526, 0.500, 90), (0.8120, 1.000, 103), (0.7448, 2.606, 141)	83.66
0.6	(0.8526, 0.500, 90), (0.8120, 1.000, 103), (0.7448, 2.606, 141), (0.6841, 5.483, 170), (0.6006, 12.374, 298)	86.50
0.5	(0.8526, 0.500, 90), (0.8120, 1.000, 103), (0.7448, 2.606, 141), (0.6841, 5.483, 170), (0.6006, 12.374, 298), (0.5566, 20.068, 325)	84.55
0.4	(0.8526, 0.500, 90), (0.8120, 1.000, 103), (0.7448, 2.606, 141), (0.6841, 5.483, 170), (0.6006, 12.374, 298), (0.5566, 20.068, 325), (0.4909, 32.860, 373), (0.4231, 48.392, 430)	86.15
0.3	(0.8526, 0.500, 90), (0.8120, 1.000, 103), (0.7448, 2.606, 141), (0.6841, 5.483, 170), (0.6006, 12.374, 298), (0.5566, 20.068, 325), (0.4909, 32.860, 373), (0.3748, 63.924, 457), (0.4231, 48.392, 430)	85.26
0.2	(0.8526, 0.500, 90), (0.8120, 1.000, 103), (0.7448, 2.606, 141), (0.6841, 5.483, 170), (0.6006, 12.374, 298), (0.5566, 20.068, 325), (0.4909, 32.860, 373), (0.3748, 63.924, 457), (0.4231, 48.392, 430), (0.2784, 95.726, 541)	82.59
0.1	(0.8526, 0.500, 90), (0.8120, 1.000, 103), (0.7448, 2.606, 141), (0.6841, 5.483, 170), (0.6006, 12.374, 298), (0.5566, 20.068, 325), (0.4909, 32.860, 373), (0.3748, 63.924, 457), (0.4231, 48.392, 430), (0.2784, 95.726, 541), (0.1792, 136.430, 672)	88.40
0.0	(0.8526, 0.500, 90), (0.8120, 1.000, 103), (0.7448, 2.606, 141), (0.6841, 5.483, 170), (0.6006, 12.374, 298), (0.5566, 20.068, 325), (0.4909, 32.860, 373), (0.3748, 63.924, 457), (0.4231, 48.392, 430), (0.2784, 95.726, 541), (0.1792, 136.430, 672), (0.0958, 175.819, 768)	86.32